Wiley
International Journal of Polymer Science
Volume 2024, Article ID 2280726, 19 pages
https://doi.org/10.1155/2024/2280726

WILEY

Research Article

Determination of Deformation Behaviors and Energy Absorption of Lightweight Composite Lattice Cylinders With Different Structures

Ilyas Bozkurt

Department of Mechanical Engineering, Architecture and Engineering Faculty, Mus Alparslan University, 49250 Mus, Turkey

Correspondence should be addressed to Ilyas Bozkurt; i.bozkurt@alparslan.edu.tr

Received 1 July 2024; Accepted 18 September 2024

Academic Editor: Antonio Caggiano

The aim of this study is to determine the crushing performance of four different composite lattice cylinder structures (hexagonal, circular, square, and triangular) under quasistatic compression loading using the finite element method. The numerical model was developed by performing *progressive damage analysis* with the *MAT-54 material model* in the *LS-DYNA* finite element software. The crushing performance (peak force (PF), mean crushing force (MCF), crushing force efficiency (CFE), and specific energy absorption (SEA)) and damage types of composite cylinders for different lattice structures, specimen thicknesses, lengths, material types and compression directions (axial and tangential) were determined and compared with results from other studies in the literature. At the end of the study, it was determined that the PCF value of the square lattice structure was 19.3% higher than hexagonal lattice structure, 37.6% higher than the circular lattice structure, and 33.4% higher than triangular lattice structure for axial loading. The AL specimen exhibited the highest EA value with 171 J, while the CFRP specimen had the highest SEA value with 4.2 J/g. The CFE value was the highest for the AL specimen. The deformation behavior of lattice cylinders varied primarily according to the cell type.

Keywords: composite lattice cylinder; compression test; finite element method; *LS DYNA*; progressive damage analysis

Summary

- The crushing performance of different composite lattice cylinder structures was examined.
- The effects of composite lattice structures on specimen thicknesses and lengths, material types, and compression directions were determined.
- The numerical model was implemented in the *LS DYNA* finite element model by performing progressive damage analysis with the *MAT-54* material model.

1. Introduction

Composite materials stand out due to their lightweight, high stiffness, wear resistance, and high thermal and chemical resistance compared to other materials [1]. However, lightweight composite lattice structures have attracted much attention, especially in the aerospace industry because they are very light and durable. Curved shapes in composite structures are used to meet these needs in aerospace due to their insulation and aerodynamic effects. Cylindrical structures are preferred because their energy absorption (EA) potential is higher than that of flat plates [2]. The safety of the driver and passengers in transportation vehicles during a collision is directly related to the EA potential. The most important function of EA components is to distribute most of the load in the event of a collision or compression. For this reason, researchers have focused on the EA capability of structures.

The main purpose of using lattice structures is to reduce the total weight of the system. Especially in metal structures, when a lattice structure is used instead of the whole volume, the total weight is significantly reduced [3]. This is very important in the aviation industry where weight is an

important influence on fuel consumption. In recent years, with the improvement of the mechanical performance of composite structures, the use of composites in applications requiring mechanical strength is increasing. It is observed that curved composite structures have become common in applications ranging from bicycle frames to vehicle and aircraft parts.

The use of lightweight composite lattice structures has increased in recent years with many different structural shapes being explored. The most commonly used ones are the tetrahedral truss [4], isogrid [5] pyramidal truss [[6, 7]], Kagome shape [8], octet truss [9], egg shape [10], Y shape [[11, 12]], and others. Since structural changes have a significant effect on mechanical performance, it is likely that different structural configurations will be investigated in future studies. These structures have become popular due to their lightweight and high strength properties. They are also used as core structures in sandwich structures and as strength enhancers in cylindrical structures [[13, 14]].

Many different tests and laboratories are needed to produce composite structures, which have a wide range of applications, to test the specimens produced and to determine their mechanical performance [10]. The limited and high cost of the materials needed in the production processes, along with the trial-and-error testing of the produced specimens using expensive testing equipment, restrict researchers [15]. Due to these high costs, researchers have carried out the production and testing stages with the help of finite element programs [16]. However, although the accuracy of finite element analysis has increased with the advances in finite element technology, the accuracy rate decreases when these analysis results are not supported by experimental work. To overcome this problem, researchers have created numerical models based on experimental studies that were previously performed at high costs and with significant difficulties. In the literature, it is evident that experimental studies that are very similar to one another are conducted at high cost, requiring significant time and labor. Instead of doing the same or similar experimental studies, it will be very convenient for researchers to create a numerical model with reference to previous studies. Since these numerical models share the same boundary and loading conditions as the experimental studies, they can yield results very close to the actual values [17].

Many studies have been conducted to evaluate the mechanical performance of cylindrical composite structures [[15, 18, 19]]. However, the number of studies investigating and comparing the mechanical performance (EA efficiency, peak crushing force (PCF), mean crushing force (MCF), and max displacement) of lightweight composite lattice cylinder structures (hexagonal, circular, square, and triangular) is limited. Wu et al. [13] investigated the structural compressive strength of sandwich cylinder structures with lattice cores under compression loading corresponding to four possible failure modes (Euler buckling, axisymmetric buckling, local buckling, and front panel crushing of sandwich cylinders). Zhang et al. [20] numerically investigated the damage mechanisms of lattice cylindrical structures. Hao et al. [21] investigated the compression behavior of an environmentally friendly natural fiber–based isogrid truss cylinder made of pineapple leaf fibers and phenol formaldehyde resin matrix. Li et al. [22] fabricated sandwich cylinders with lattice cores and investigated their compression behavior. Zheng et al. [5] theoretically analyzed the structural stiffness and critical axial force of lattice cylinders by the equivalent continuity method. They investigated spherical buckling, out-of-plane strut buckling, in-plane strut buckling, in-plane strut buckling, and strength fracture damage of the lattice structure under load. Wu et al. [[13, 23]] theoretically and experimentally investigated the compression and shear behavior of sandwich cylinders with low-density pyramid lattice cores made of plain woven carbon fiber fabrics. Golivari et al. [24] investigated the EA parameters of bolted double hat connections reinforced with adhesive bonding method. Mahmoodi, Shojaeefard, and Saeidi Googarchin [25] investigated the crashworthiness behavior of tapered multicellular tubes theoretically and numerically. Tapering of the side walls and division of the cross section into cells were used to improve the EA of the thin-walled structure. Saeidi Googarchin et al. [26] investigated the EA properties of conical multicellular tubes cured with foams. Khorasani and Saeidi Googarchin [27] theoretically and numerically investigated the crashworthiness characteristics of conical structures with uniform cells in cross-section when subjected to oblique impacts. Li et al. [28] investigated the behavior of honeycomb sandwich cylinder structures fabricated by a winding-based method under compressive load. Hajjari et al. [3] fabricated a lattice composite cylinder made of hexagonal unit–cell lightweight E-glass yarn using a textile–based method and investigated the impact resistance performance and quasistatic axial compression behavior experimentally and numerically.

In this study, the crushing performance of different shaped glass/epoxy lightweight composite lattice cylinder structures (hexagonal, circular, square, and triangular) under quasistatic compressive loading was determined using the finite element method. A previous experimental study was used to support the numerical model. The numerical model was developed by performing progressive damage analysis with *MAT-54* material model in *LS DYNA* finite element model. Using the numerical model supported by the experimental study, the crushing performance (peak force (PF), MCF, crushing force efficiency (CFE), and specific energy absorption (SEA)) of composite cylinders for different composite lattice cylinder structures, specimen thicknesses, specimen lengths, material types, and compression directions (axial and perpendicular to the axis) and the types of damage occurred were determined. At the end of the study, the crushing performance was compared. In addition, SEA performance was compared with studies in the literature.

2. Materials and Method

2.1. Experimental Study. It is important that the numerical model used in the study is supported by an experimental study in order to ensure accurate results. Therefore, in this study, the numerical model was created by referencing the experimental study in Ref. [29]. In the study, cylinder

specimens were produced by filament winding process using E-glass/PET 199. The cylinder was wound using 20 layers of E glass/PET 199 with a stacking sequence of $[\pm 75]_{10}$. Specimens have a length of 100 mm, an inner diameter of 80 mm, and a wall thickness (t_s) of 2.4 mm. The specimens were axially compressed under quasistatic loading condition. The displacement rate of the axial compression test was 2 mm/min. The experimental tests were repeated five times each.

To determine and compare the EA capabilities of composite lattice cylinders, it is necessary to calculate the crashworthiness parameters. These parameters are calculated from force-displacement curves. Figure 1 shows an example force-displacement curve obtained from a compression test.

The load first rises to a maximum point and then drops sharply, followed by the formation of folds in the structure. The process continues with an average crushing force until all energy is absorbed. Here; the area under the graph gives the absorption energy (AE) or total internal energy (TIE) (1).

$$\mathrm{EA}(\mathrm{dx}) = \int_0^{d_x} F(x)\mathrm{dx} \tag{1}$$

where d_x is the crush distance and $F(x)$ is the crush force as a function of the crush distance of x.

$$\mathrm{SEA} = \frac{\mathrm{EA}}{m} \tag{2}$$

Energy per unit of mass is denoted by SEA, where m is mass.

CFE is the ratio of the average crushing force (F average) to the PCF and is defined as

$$\mathrm{CFE} = \frac{\mathrm{MCF}}{\mathrm{PCF}} \tag{3}$$

The PCF is the maximum force value of the system. The MCF is considered as the average force. In this study, the effective crushing distance for all specimens was set to 75% of the original cylinder length.

2.2. Numerical Study

2.2.1. Finite Element Model. Many finite element software programs such as *ANSYS*, *ABAQUS*, *NASTRAN*, and *LS-DYNA* are used to model the behavior of composite structures under load. Among these software, *LS-DYNA* stands out with its comprehensive material models in the material library, complex contact condition definition features, and solution algorithms. Therefore, *LS-DYNA* software was preferred in this study to determine the compression behavior of composite specimens [30]. *LS-DYNA* helps approximate the compression-induced damage of composite pipes and allows the development of new models by modifying these models. The solution technique of the program includes material cards that provide damage models based on the continuous damage mechanism (CDM).

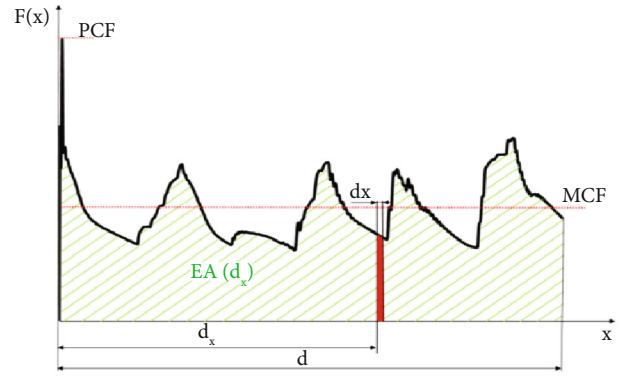

Figure 1: Example of the force-displacement curve obtained from compression test.

According to these selected material cards and damage criteria, the material exposed to a load up to a certain critical threshold value is damaged after a while. The specimen was modeled as a shell element with a mesh size of 2.5 mm × 2.5 mm and 20 integration points. The number of meshes is a very effective parameter in finite element analysis time and closeness to experimental results. Therefore, a 2.5 × 2.5 mm mesh structure was used to obtain results close to the experimental results, for efficiency and fast solutions. Figure 2 shows the compression test finite element model of the composite pipes.

The specimens were placed between the upper and lower rigid plates. The lower plate movements were kept fixed in the x, y, and z directions, while the upper plate was allowed to move freely in the z direction. The compression speed of the top plate was set at 1.5 m/s considering the processing time and efficiency. "CONTACT_AUTOMATIC_SURFACE_TO_SURFACE" contact card was defined between the top plate and the composite. "CONTACT_AUTOMATIC_SINGLE_SURFACE" contact card was used to prevent interference between the elements in the composite specimen. Both dynamic and static friction coefficients were defined as 0.2 [31]. For the quasistatic compression test of the composite specimens, the upper plate was moved in the z-direction using the BOUNDARY_PRESCRIBED_MOTION_ SET card. The bottom plate was assigned as fixed. To avoid dynamic effect, the initial velocity was increased linearly starting from 0 up to 1.5 m/s and then kept constant.

The four different lattice structures used in the study are shown in Figure 3. The most important research novelty of this study, unlike other studies in the literature, is the determination and comparison of the crushing performance of these four different lattice structures. Although there are many cage structures in the literature, it has been observed that the compression behavior of these four structures has not been compared. With the advancement of technology and the development of manufacturing techniques, it is possible to produce composites with many different structures. Researchers have focused on new structures with lighter weight and higher strength. Another important point that makes this study important is to produce very light and high-strength structures. Therefore, determining the

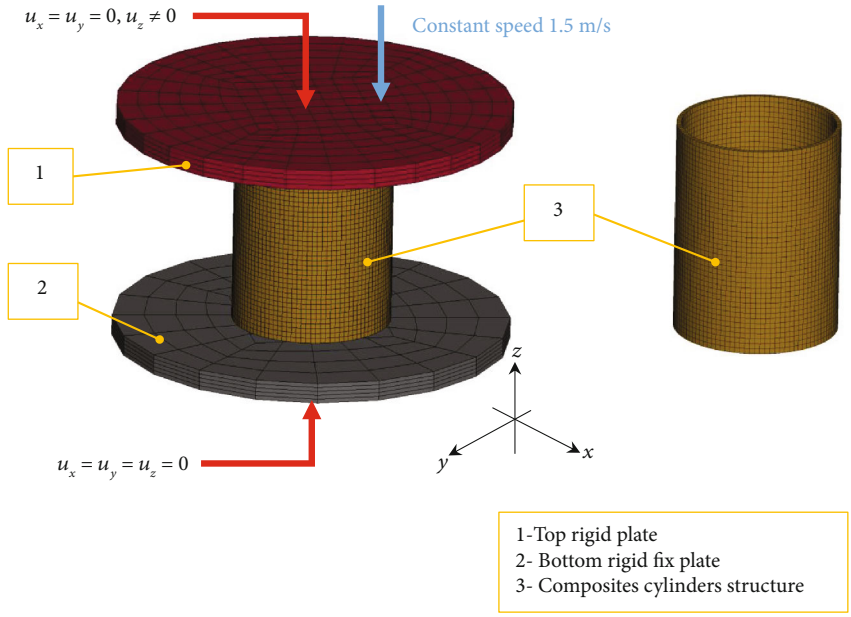

Figure 2: Mesh model generated for compression simulations of the composites circular cylinder specimens.

performance of these new structures will be an important reference source for researchers working in this field. The reaction of the material under load may vary with the change in structural configurations. Therefore, the compression performance of these structures subjected to the same compression load under the same boundary conditions will be determined in detail. There are holes in the lattice structures used. Therefore, relative density is used to describe the amount of material used per unit. Relative density is determined by dividing the area of the cell walls used in a cell by the total area of the unit cell. The way of calculation varies according to the cell type. Relative density calculation formulas are given in Table 1. Relative density values of the lattice structures used in the study are given in Table 2 [10]. In the dimensions given in the table, L_c, L_s, and t_c represent cell length, specimen length, and cell thickness, respectively.

2.2.2. Material Models. The determination of the material model is of great importance for the finite element model results to closely match the experimental results. In the *LS-DYNA* finite element program, there are many material models to describe composite materials. Among these, *MAT-22*, *MAT-54/55*, *MAT-58*, *MAT-59*, and *MAT-162* are the most commonly used material models by researchers. The main differences between these material models are the damage criterion and material behavior as a result of loading. Strength parameters (transverse compressive strength, longitudinal compressive strength, transverse tensile strength, and shear strength) are used to determine when the material is damaged. Load calculation in a material occurs in three stages. (1) Stress concentration points and strain distributions are determined. (2) The maximum load due to the load is calculated. (3) The material is damaged according to the damage mode used. *MAT-22* includes four damage modes (matrix tensile mode, matrix compression mode, fiber tensile mode, and fiber compression mode), while *MAT-54* considers three damage modes (tensile fiber, tensile matrix, and compression matrix mode). *MAT-55* differs from *MAT-54* as it is based on the Tsai–Wu criterion for matrix damage. *MAT-58*, which is based on stress at fracture surfaces, stands out with its *SLIMx* feature that describes the interaction between layers from damage. *MAT-59* is an elastic-plastic material model that can also predict compression and shear through thickness. The *MAT-162* model offers the capability to investigate the postload damage in composite structures in three dimensions (3D). In this study, the *MAT-54* material model was preferred. This choice was made because *MAT-54* is highly compatible with shell elements, lacks complex damage parameters, has a damage model that effectively describes the damage mechanisms of composite structures (Chang–Chang and Tsai–Wu), is widely referenced in the literature, and offers short analysis times. When defining the *MAT-54* material model, 25 input values are needed. Of these, 15 parameters are the material constants given as shown in Table 3. The remaining 10 numerical parameters (shown in Table 4) are obtained by calibrating through finite elements [32]. Mechanical properties of Al 6061-T6 are given in Table 5. The indices a, b, and c in the table represent the fiber directions. Some parameters used in the MAT54 material model are determined by experimental tests, while others are determined by trial-and-error method. Therefore, a comprehensive study is required for the calibration of these parameters [33].

2.2.3. MAT_54-55: Enhanced Composite Damage Model. It is the most widely used material model together with shell elements in the analysis of composite structures. In the material model, it is assumed that the material is orthotropic and linear elastic in the absence of any damage. In this model, *MAT-54* damage criterion was proposed by Chang, and *MAT-55* damage criterion was proposed by Tsai–Wu. This material model has the same operating logic as *MAT-22*

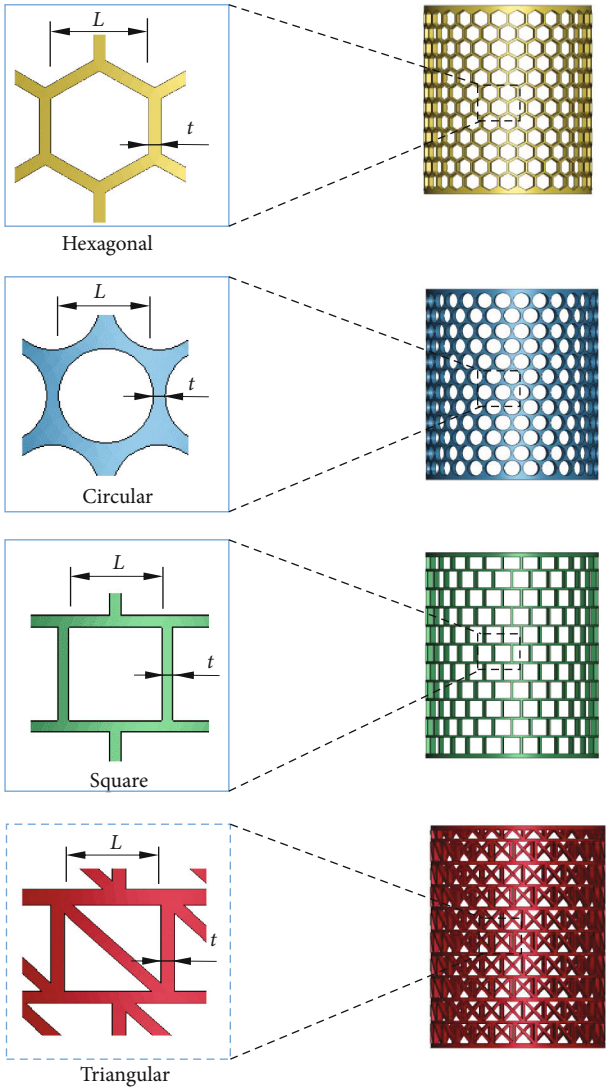

Figure 3: Types of lattice structure used in the study.

but includes an additional compression damage mode. The Chang–Chang criterion (*MAT-54*) is given below.

Tensile fiber ($\sigma_{11} > 0$).

$$\left(\frac{\sigma_{11}}{S_1}\right)^2 + \bar{\tau} = 1 \tag{4}$$

All moduli and Poisson's ratios are set to zero when the tensile fiber failure criteria are met, that is, $E_1 = E_2 = G_{12} = \upsilon_{12} = \upsilon_{21} = 0$. All the stresses in the elements are reduced to zero, and the element layer has failed.

Failure mode for compressive fiber ($\sigma_{11} > 0$)

$$\left(\frac{\sigma_{11}}{S_{12}}\right)^2 = 1 \tag{5}$$

Table 1: Relative density calculation formulas of truss structures.

Cell name	Cell shape	Relative density ($\bar{\rho}$)
Hexagonal	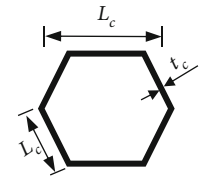	$\left(\frac{2}{\sqrt{3}}\right)\frac{t_c}{L_c}$
Circular	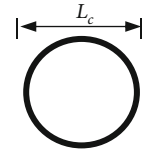	$\frac{4t(L_c - t_c)}{L_c^2}$
Square	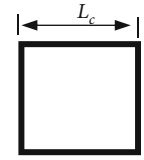	$2\frac{t_c}{L_c}$
Triangular	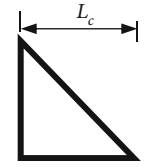	$\left(1+\sqrt{2}\right)\frac{t_c}{L_c}$

Failure mode for tensile matrix ($\sigma_{11} > 0$)

$$\left(\frac{\sigma_{22}}{S_2}\right)^2 + \bar{\tau} = 1 \tag{6}$$

Failure mode for compressive matrix

$$\left(\frac{\sigma_{22}}{2S_{12}}\right)^2 + \left[\left(\frac{C_2}{2S_{12}}\right) - 1\right]\frac{\sigma_{22}}{C_2} + \bar{\tau} = 1 \tag{7}$$

where E_1 and E_2 are the longitudinal and transverse elastic moduli, respectively, G_{12} is the shear modulus, υ_{12} and υ_{21} are the in-plane Poisson's ratios. When damage occurs in the composite layers (through the thickness with Integration points), elements are deleted here. Elements that have nodes in common with the deleted elements can be reduced in strength using the SOFT parameter.

3. Results and Discussion

The load-displacement graph of the glass composite circular cylinders, obtained under axial load, is shown in Figure 4. Upon analysis, it is evident that the numerical results closely match the experimental results. The PFC value of the composite circular specimen is 68.8 kN in the experimental study and 69.06 kN in the finite element result. The difference between the experimental and numerical results is 0.37%. The MCF value was determined to be 34.5 kN in the experimental results and 33.25 kN in the numerical results. The

Table 2: Characteristics of the lattice structures used in the study.

Name	Cell type	L_c (mm)	t_c (mm)	L_s (mm)	Relative density
H6	Hexagonal	6	1	100	0.33
H8	Hexagonal	8	1	100	0.25
H12	Hexagonal	12	1	100	0.16
C6	Circular	6	1	100	0.55
C8	Circular	8	1	100	0.43
C12	Circular	12	1	100	0.30
S6	Square	6	1	100	0,33
S8	Square	8	1	100	0.25
S12	Square	12	1	100	0.16
T6	Triangular	6	1	100	0.40
T8	Triangular	8	1	100	0.30
T12	Triangular	12	1	100	0.20

difference between the experimental and numerical results is 3.60%. Under the effect of compression force, the load reaches the maximum point. Then, crushing and fracture damages occur in the composite structure [10]. These damages typically occur at the contact point between the top plate and the composite cylinders. In finite element analysis, the elements at this contact point are deleted due to the high stress [30]. These damages are reflected as a sudden load drop in the PF-displacement graph. The deformation patterns that cause the initial damage and the subsequent force drop are depicted both experimentally and numerically. After the initial damage, the force continues to hover around the mean crushing load until the end of the compression process. The experimental and numerical data have a serrated shape with ups and downs. The upward sloping sections in the experimental data represent an increase in the stresses on the elements and an increase in the resistive load due to multiple crack propagation. It can be observed that the force decreases negatively as the loading condition continues. In finite elements, an upward increase occurs in the graph due to loads on the element reaching a certain stress value or strain rate. When the critical stress value is reached, sudden deletion occurs in the element. Therefore, the load is wasted and a decrease in the force value occurs. Here, when this stress value between the layers reaches the critical value, MOD-I delamination may also occur and cause load drop [34]. When the oscillations in the numerical results are carefully examined, it is observed that they have different amplitudes and ranges from the experimental results.

Here, amplitude and wavelength are related to the material model used. In the numerical model, the sudden drop after the peak load and the large oscillation that occurs afterwards is observed as softer in the experimental study. This is because, even if the elements in contact with the plate applying compression force are crushed and damaged, the force does not decrease at the point of contact since the damaged area and the upper plate continue to be in contact. In the numerical model, however, the sudden deletion of the elements in contact with the upper plate causes a discharge in the force. This causes sudden and sharp drops.

Composite structures can be exposed to very different loads depending on the sector and application areas. Composite structures exposed to load show resistance to this applied load in proportion to their mechanical properties. Therefore, it is necessary to know the strength values of composite structures according to their application areas. In general, metal materials react as elongation or shortening when exposed to load. They are then damaged by plastic deformation. However, composite structures can be damaged in many different damage modes [35].

Therefore, composites exposed to compression test can absorb this energy through damage mechanisms such as matrix cracking, delamination, and fiber breakage. These damage types were observed in the specimens at the end of the compression test. The behavior of the composite specimen under compression load is shown progressively in Table 6. The deformation pictures for the experimental study were taken from Ref. [29] for comparison. The first deformation occurred at the point of contact between the top plate and the composite pipe, in alignment with the experimental study. Then, the damage size progressed as the compression force continued. The initial damage point depends on the orientation angle of the fibers for composite structures [10]. The arrangement of the fibers, which is the biggest factor in providing strength in the structure, is very important at this point. To absorb the energy generated by the compression effect, metal structures generally react with folding, bending, and then plastic deformation. In composite structures, matrix cracking, fiber bending, transverse shear, and delamination absorb this energy.

Table 7 shows the deformation pictures under load and the stress values on the structure. In the finite element working principle, the structure is divided into small elements, and stress is calculated. In order for an element to be deleted or deformed, it must be subjected to a certain load value. If the load to which it is exposed is greater than the maximum strength limits, deformation or deletion occurs in that element. Therefore, the stress data of the structure are important for understanding the overall condition of the system.

Table 3: Mechanical parameters of the GFRP [25] and CFRP [10] composite.

Symbol	Property	CFRP [10]	GFRP [26]	Unit
ρ	Density	1500	2000	kg/m^3
E_a, E_b	Young modulus a and b direction	43.7	37.9	GPa
E_c	Young modulus in c direction	14.57	11.5	GPa
υ_{ab}	Poisson's ratio in ab plane	0.21	0.29	—
υ_{bc}	Poisson's ratio in bc plane	0.21	0.29	—
υ_{ca}	Poisson's ratio in ca plane	0.21	0.29	—
G_{ab}	Shear modulus in ab plane	14.18	4.5	GPa
G_{bc}	Shear modulus in bc plane	14.65	4.5	GPa
G_{ca}	Shear modulus in ca plane	14.65	4.5	GPa
S_{aT}	Tensile strength a direction	0.589	0.936	GPa
S_{aC}	Compressive strength a direction	0.1096	0.484	GPa
S_{bT}	Tensile strength b direction	0.589	0.025	GPa
S_{bC}	Compressive strength b direction	0.1096	0.143	GPa
S_{ab}	Shear strength in ab plane	0.1082	0.0161	GPa

Table 4: Failure parameters of the composite.

Symbol	Description	Unit
DFAILM	Transverse matrix failure strain experimental	0.0
DFAILS	Shear failure strain experimental	0.0
DFAILT	Tensile fiber failure strain experimental	0.0
DFAILC	Compressive fiber failure strain experimental	0.0
TFAIL	Timestep for element deletion computational	0.16
Alpha	Shear stress parameter damage dependent	0.0
Soft	Strength reduction factor damage dependent	0.7
FBRT	Reduction factor for S_{aT} damage dependent	1
YCFAC	Reduction factor for S_{aC} damage dependent	3
EFS	Effective failure strain computational	0.90

Table 5: Mechanical properties of Al 6061-T6.

Density (kg/m^3)	E (GPa)	Poisson ratio	Yield stress (MPa)	Failure strain
2850	72	0.33	252	0.4

The finite element model was supported with experimental data to achieve high accuracy. Using this model, results with high accuracy rates can be obtained by making modifications to specimens with different structural configurations, material types, and mechanical properties [31]. With advancing technology, researchers have achieved high accuracy rates by using finite element technology under the same boundary conditions, rather than performing high-cost, time-consuming, and challenging experiments [32, 33].

Finite element technology can also be used to assess the feasibility of high-cost tests before implementing them. This model is particularly widely used in the aerospace industry, where costs are very high. Therefore, advances in this field and the number of studies in this field have increased considerably in the last 10 years [36].

Using the numerical model validated by the experimental study, different lattice cylinder shell specimens were subjected to compression tests in the axial direction, and their mechanical behavior was investigated. Figure 5(a) shows the PF-displacement plots of these specimens. In Figure 5(b), the PF values of all specimens are compared. In Figure 5(a), it can be observed that the difference between the PCF and the MCF is large because the specimens have a lattice structure. Therefore, to better illustrate this force difference, it is shown in the 1 mm compression test graph. For all specimens, it is observed that after the compression load is applied, the force value rises to the peak and then drops sharply. It is then observed that it continues with an average value until the end of the test. Since the legs of the square specimen contacting the upper and lower holder were thin, damage occurred after the peak point and the force value became zero due to the damage. Then, an increase in force occurred again. When the PF results for four different lattice structures are examined in Figure 5(b), it is observed that the highest PF value is obtained for $L = 6$ mm in each lattice structure. It was observed that the PF value decreased as the L dimension increased for all four lattice structures. When compared with each other, the highest PF value was obtained as 18.36 kN for the specimen with a square-shaped lattice structure. However, the largest decrease in force with a change in L dimension was 41.65% for the square lattice structure specimen (18.36 kN for $L = 6$, 10.71 kN for $L = 12$). It was observed that the change in PF value with the change of L size in the circular lattice structure was much less than in the other lattice structures. The PF value for H6 is smaller than for S6. The wall thickness of the S6 specimen is not constant like H6. Due to the

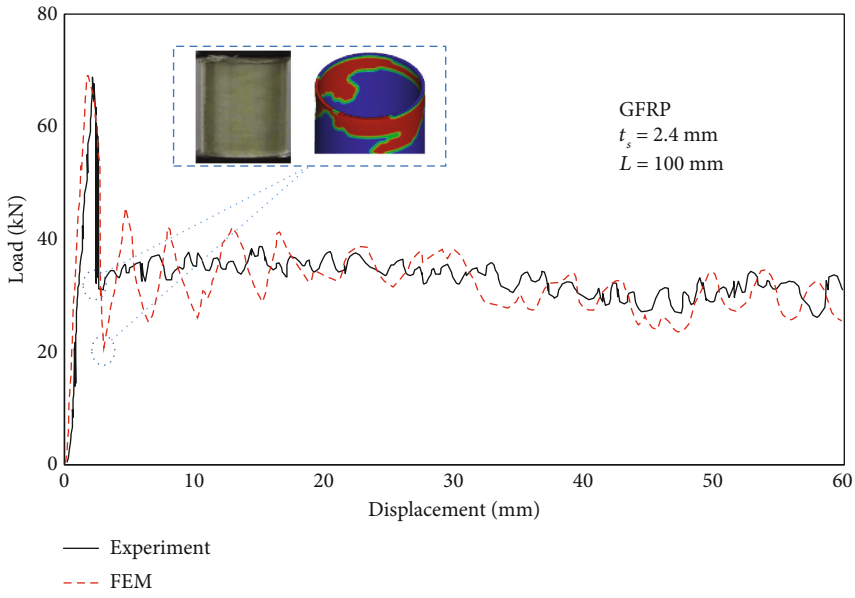

Figure 4: Quasistatic load–displacement curves for glass/epoxy composite pipes.

Table 6: Gradual damages occurring in the specimens after the compression test.

FEM	EXP	FEM	EXP
		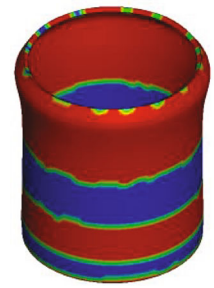	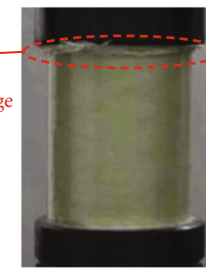
0		First damage	12.5 mm
			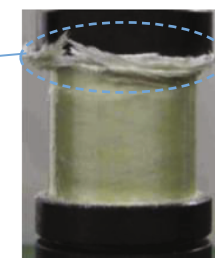
25 mm			37.5 mm
			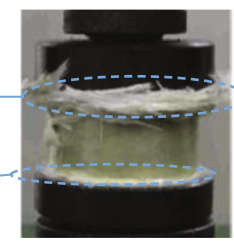
50 mm			75 mm

Table 7: Compression behavior of the specimen at different stages in FEM.

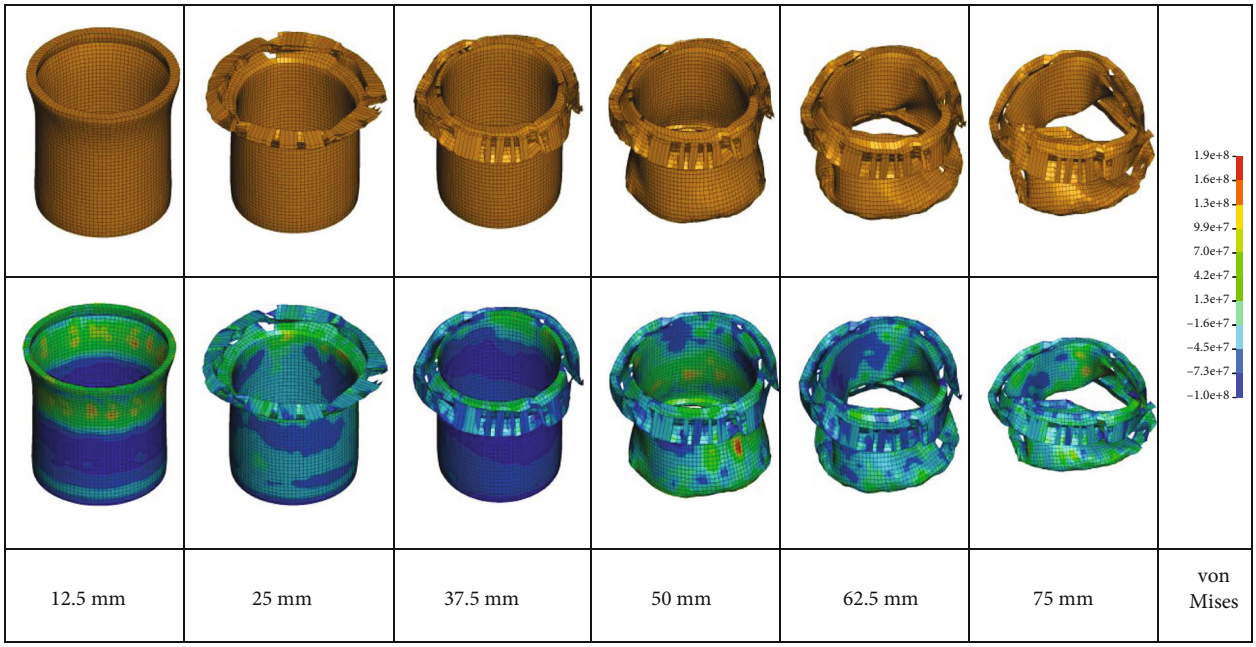

structural difference, it provides an advantage to the S6 specimen. However, when the cell length is longer, the flexibility increases. Therefore, the PF value of the S12 specimen is lower than H12. The PF change value between $L = 6$ and 8 mm decreased by 5.8%. In the triangular lattice structure, the PF value between $L = 6$ and 8 mm is 12.43 kN and 12.35 kN, respectively, while this value is 10.34 kN when $L = 12$ mm. While a gradual decrease in parallel with the length is expected, the material reaction may not show linearity under the same boundary conditions. On the other hand, such a result is actually expected because the internal dynamics of composite structures are not linear like those of metals, and there are many partially interdependent factors. The behavior of an aluminum pipe under compression load can be predicted due to its material structure. However, in composite structures, factors such as fiber type, number of fibers, matrix type, and matrix fiber compatibility. Because of this complexity, unexpected deviations can occur between the results.

Composite structures can be subjected to loads of very varying magnitudes and directions depending on the area of use. Therefore, it is extremely important to know the loads and loading patterns that the structure may be exposed to in advance and to determine the strength values of the structure in all directions in terms of engineering and design. Composite lattice cylinder structures were subjected to tangential quasistatic compression loading, and their strength values and mechanical behaviors were investigated. When Figure 6 is examined, it is observed that the highest PF value among all specimens is 24.5 kN in the T6 specimen. The lowest value occurred in the S12 specimen. When the graph is carefully examined, the highest PF result was obtained for $L = 6$ mm for each specimen group as in the compression test performed in the axial direction. This is related to relative density. As the relative density value decreases, the effect of the structure against the load decreases. The triangular lattice structure has the highest PF change with the change of L. When L increased from 6 to 12 mm, the PF value decreased by 55.9%. Similarly, it was determined that the change in PF value with the change in L length was 43.9% for hexagonal lattice structure, 27.8% for circular lattice structure, and 31.8% for square lattice structure.

Composite lattice cylinder structures can have different lengths. The effects of length on PF were analyzed and the results are given in Figure 7. The specimen nomenclature here is indicated by adding L in front of the specimen length. For example, the specimen H6-L50 represents a hexagonal lattice structure with a cell width of 6 mm and a length of 50 mm. For the four different lattice structures, the highest PF values occurred in the specimens with the shortest length ($L = 50$ mm). It was observed that the PF value decreased as the length of the structure increased [15]. The highest PF value among the four specimens occurred in the square (S6-L50) specimen with 19.6 kN. In the square specimen, the PF change with the change of L length ($L = 6$, $L = 12$) is the largest with 50.5%. This indicates that specimen size has a significant effect on PF [15].

When the behavior of structures under load is examined, it is well-known that the material type and its mechanical properties have a significant effect [37]. The reaction of materials when they are exposed to load can be different. For example, when a tensile test is applied to a ductile material such as aluminum, elongation first occurs in the specimen. After a critical threshold, plasticization and then fracture occur. There is a linear relationship between the load and the structure, allowing for easy prediction of the material's behavior due to this parallelism. But the situation is different in composite structures. In composite structures

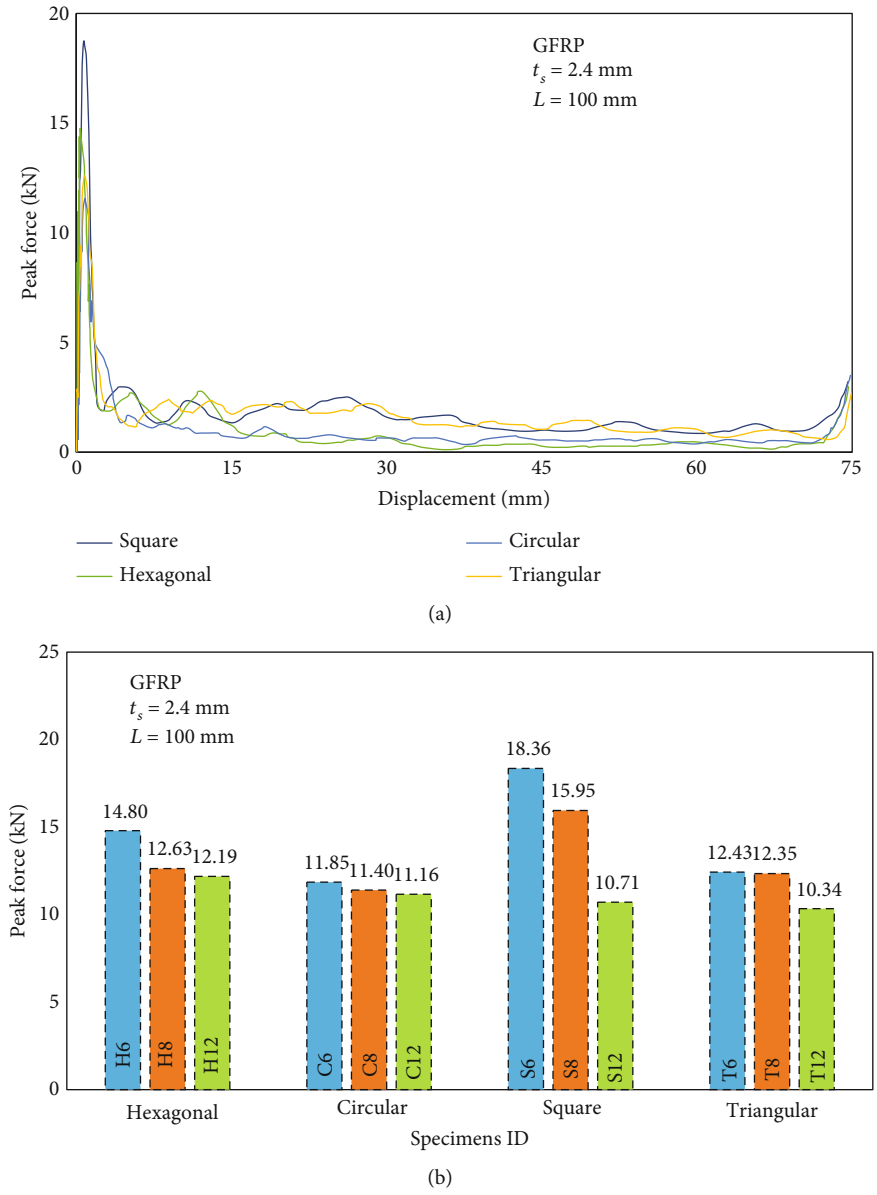

Figure 5: After axial compression (a) peak force displacement and (b) PCF graph for all specimens.

with a brittle structure, elongation occurs very little compared to aluminum structures, and a sudden failure is observed. Upon impact, the composite structure reacts based on various factors, such as the type of fiber within the composite, orientation angle, compatibility with the matrix, type of matrix, and mechanical properties. Therefore, it is not easy to predict the reaction of the composite structure under load. The peak load values of composite lattice cylinders under compression load for GFRP, CFRP, and aluminum are given in Figure 8.

When naming the specimen, the type of material used is added next to it. For example, H6-GFRP refers to a glass composite hexagonal structure with a cell width of 6 mm. Four different lattice structures are grouped accordingly. When the graph is analyzed, the highest peak load value occurred in the S6-AL specimen and the lowest in the T12-GFRP specimen. With the use of AL material in the H6 specimen, the PF value is 20.4% higher than GFRP and 17% higher than CFRP. When the graph is examined in general, it is observed that the peak load values for the lattice cylinder structures of the composite structures against aluminum are low. In composite structures, it is the fibers that provide the main strength in the system. The shortness of the fiber structures due to the lattice design significantly affects the strength value [38].

The effects of material thickness on PF are shown in Figure 9. PF values for material thickness (1.2, 2.4, and 4.8 mm) are given for all specimens. It is observed that the PF value increases in parallel with the increase in material thickness for all lattice types. The highest peak load value among all lattice structures occurred in the H8-4.8 specimen with hexagonal structure.

The performance of energy-absorbing structures is crucial to protect people or property from damage in the event of impact. Experts conducting research in this field

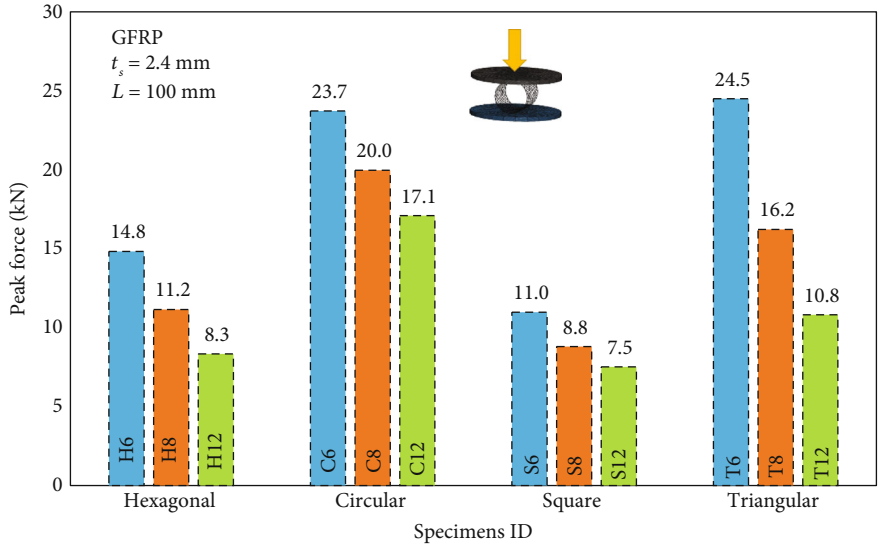

Figure 6: PF graph after tangential compression.

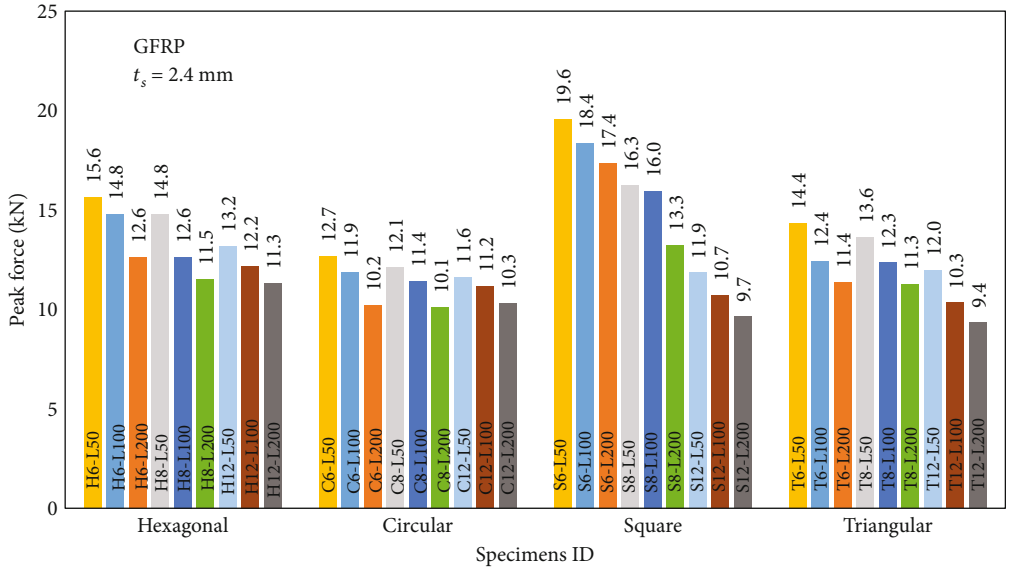

Figure 7: Effect of length on peak force after axial load.

evaluate the situation in the context of cost-benefit while designing. For example, in the aviation industry, lattice structures with low density and high EA potential are preferred. Because it is predicted that fuel consumption will be minimized due to their lightweight. Therefore, it is an important choice that will reduce the rate of carbon emissions. In the literature, some parameters are evaluated by taking some parameters to determine the EA potential. These are PCF, MCF, SEA, and CFE parameters. These parameters and the calculation method are mentioned in detail in the previous section. The summary result of the study is given in Table 8.

EA is calculated by calculating the area under the force-displacement graph. But the value calculated here is the energy absorbed by the total weight. To find the absorbed energy per unit, SEA is obtained by dividing the total energy by the total mass. In the aircraft industry and the automobile sector, the SEA value is taken into account more, because lighter weight but more EA is demanded. ES and SEA values of all specimens are given in Figure 10. When Figure 10(a) is examined, it is observed that the EA value changes as the material type changes. In hexagonal, square, and triangular specimens, the EA value decreases as the L dimension increases for all materials. But in circular specimen, it increases on the contrary. Here, the cell wall of the circular structure is different from the other three types. In the other three structures, the cell wall is the same thickness, whereas in the circular structure, it is the same only in the middle part. Due to the circular shape, the middle part and the upper part are different from each other. However, when

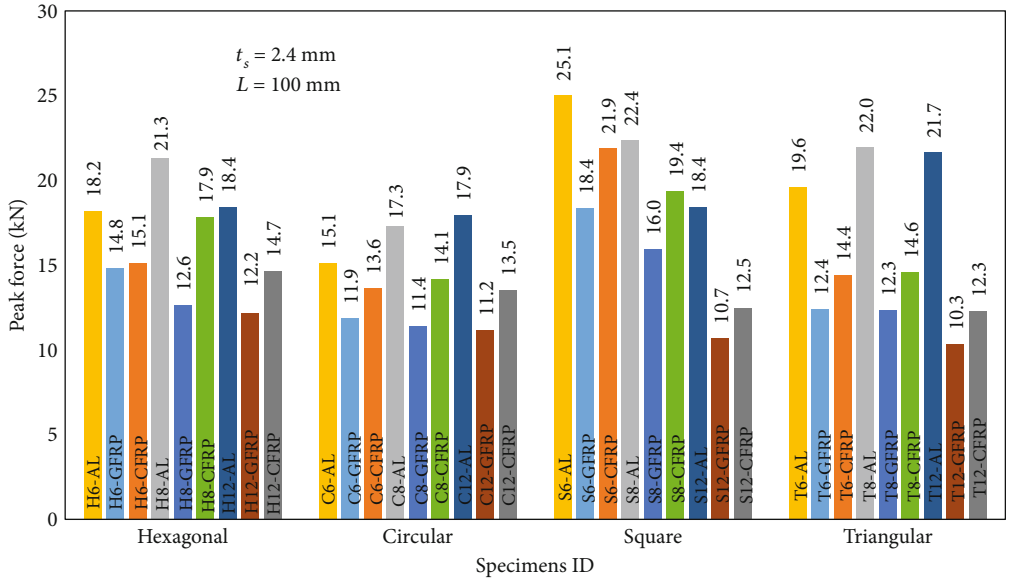

FIGURE 8: Effect of material on peak force.

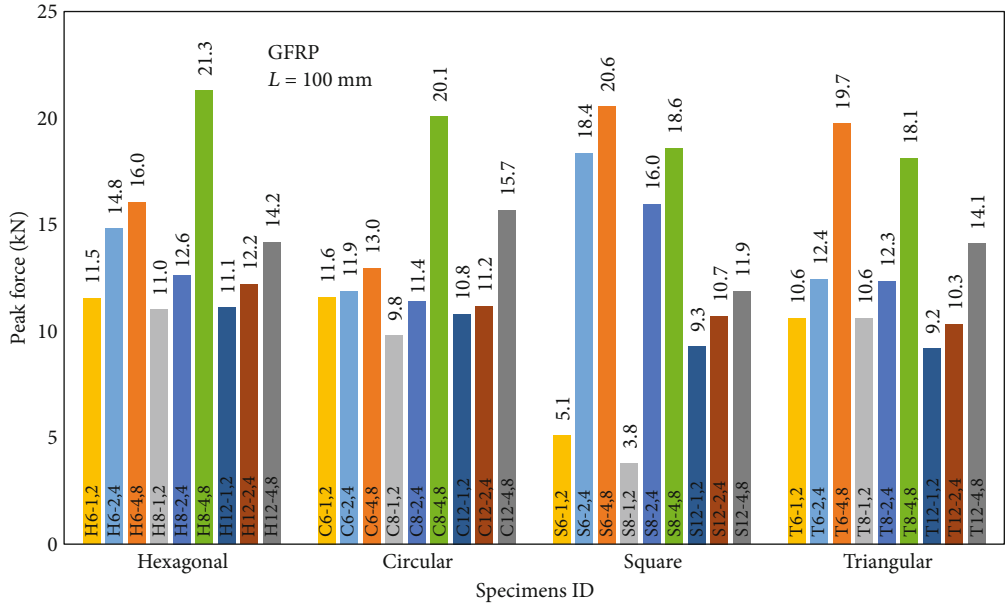

FIGURE 9: Effect of thickness (t_s) on peak force.

SEA values are analyzed in Figure 10(b), it is observed that C12-CFRP is higher than C12-AL. The main reason for this is the high density of AL material. Even if the relative density values are the same, the density has a great effect on the weight. In addition, the SEA value in the compression test of the solid circular tube was determined as 16.82 J/g [29]. The four different structures used in the study did not reach this value.

When the highest PCF values according to the material type are examined, it determined the T6 specimen with 65.9 kN and 122.3 kN in GFRP and CFRP, respectively, and the C12 specimen with 171 kN in AL. Therefore, it is observed that the type of lattice is an impressive parameter on the EA [39]. Even though the EA of aluminum structures was higher than composite GFRP and CFRP, the SEA value was lower than CFRP. The reason why it is higher than GFRP is that the density of the composite used is higher than carbon. Since the density of aluminum is high, that is, the weight efficiency is low, the SEA value decreases by dividing the total energy by the total mass. In order to prevent this situation, researchers have aimed to increase efficiency by conducting research in hybrid structures where aluminum and composite structures are combined [13, 39]. In addition, the amount of energy absorbed can be increased

Table 8: Summary of the results.

	Type	L (mm)	ID	m (g)	t (mm)	EA (J)	SEA (J/g)	PFC (kN)	MCF (kN)	CFE
GFRP	Hexagonal	6	H6	31.6	2.4	17.2	0.5	12.63	0.23	0.018
		8	H8	28.4	2.4	12.3	0.4	14.80	0.16	0.011
		12	H12	25.5	2.4	7.3	0.3	12.59	0.10	0.008
	Circular	6	C6	33.7	2.4	32.1	1.0	11.45	0.43	0.037
		8	C8	36.6	2.4	44.8	1.2	11.40	0.60	0.052
		12	C12	34.0	2.4	59.8	1.8	11.36	0.80	0.070
	Square	6	S6	31.5	2.4	17.4	0.6	18.36	0.23	0.013
		8	S8	25.6	2.4	9.7	0.4	15.95	0.13	0.008
		12	S12	21.5	2.4	6.1	0.3	10.71	0.08	0.008
	Triangular	6	T6	53.5	2.4	65.9	1.2	12.23	0.88	0.019
		8	T8	43.8	2.4	24.8	0.6	12.35	0.33	0.010
		12	T12	32.1	2.4	9.9	0.3	10.34	0.13	0.008
AL	Hexagonal	6	H6	48.6	2.4	60.7	1.3	18.20	0.81	0.044
		8	H8	43.7	2.4	38.8	0.9	21.30	0.52	0.024
		12	H12	39.2	2.4	22.5	0.6	18.44	0.30	0.016
	Circular	6	C6	51.8	2.4	95.7	1.8	15.15	1.28	0.084
		8	C8	56.3	2.4	160.9	2.9	17.30	2.15	0.124
		12	C12	52.3	2.4	171.2	4.1	17.93	2.28	0.127
	Square	6	S6	48.4	2.4	45.1	0.9	25.05	0.60	0.024
		8	S8	39.4	2.4	48.2	1.2	22.37	0.64	0.029
		12	S12	33.1	2.4	13.8	0.4	18.45	0.18	0.010
	Triangular	6	T6	82.3	2.4	196.7	2.4	19.60	2.62	0.134
		8	T8	67.3	2.4	99.7	1.5	21.95	1.33	0.061
		12	T12	49.4	2.4	30.0	0.6	21.67	0.40	0.018
CFRP	Hexagonal	6	H6	27.1	2.4	29.6	1.1	15.13	0.40	0.026
		8	H8	24.4	2.4	21.4	0.9	17.85	0.28	0.016
		12	H12	21.9	2.4	12.8	0.6	14.67	0.17	0.012
	Circular	6	C6	28.9	2.4	52.2	1.8	13.63	0.70	0.051
		8	C8	31.4	2.4	87.7	2.8	14.15	1.17	0.083
		12	C12	29.1	2.4	121.2	4.2	13.55	1.62	0.119
	Square	6	S6	27.0	2.4	24.5	0.9	21.93	0.33	0.015
		8	S8	22.0	2.4	14.9	0.7	19.37	0.20	0.010
		12	S12	18.5	2.4	9.3	0.5	12.49	0.12	0.010
	Triangular	6	T6	45.8	2.4	122.3	2.7	14.41	1.63	0.113
		8	T8	37.5	2.4	50.5	1.3	14.60	0.67	0.046
		12	T12	27.5	2.4	16.3	0.6	12.29	0.22	0.018

by using high-performance aluminum alloys. For composite structures, fiber orientation and fiber arrangement have a significant effect on EA [40].

The PCF value is an important parameter for assessing crashworthiness. However, the most important parameter affecting the EA capacity is MCF. In some cases, the PCF value may be too high while the MCF value may be too low. Therefore, the higher the MCF value, the higher the EA capacity. The CFE value represents the efficiency between these two. It should be as high as possible to maximize EA efficiency without causing damage during an accident. The PCF, MCF, and CFE values for GFRP, CFRP, and AL materials for all specimens are given in Figure 11. When Figure 11(a) is analyzed, it is observed that the highest PCF value occurs in AL material in specimen S6. Therefore, it is observed that the material type has a significant effect. It is observed that the PCF of the square lattice structure is the highest for all three materials. Although the PCF value is high for the square lattice structure, Figure 11(b) shows that the MCF value is low, and therefore, the EA efficiency is also low for the CFE. The PF value of CFRP is higher than GFRP due to its mechanical performance. The highest CFE value for all material types was the C12 specimen.

The deformations of the truss structures are given in Figure 12. After the load is applied to the truss structure, it gradually increases with the displacement, and no significant

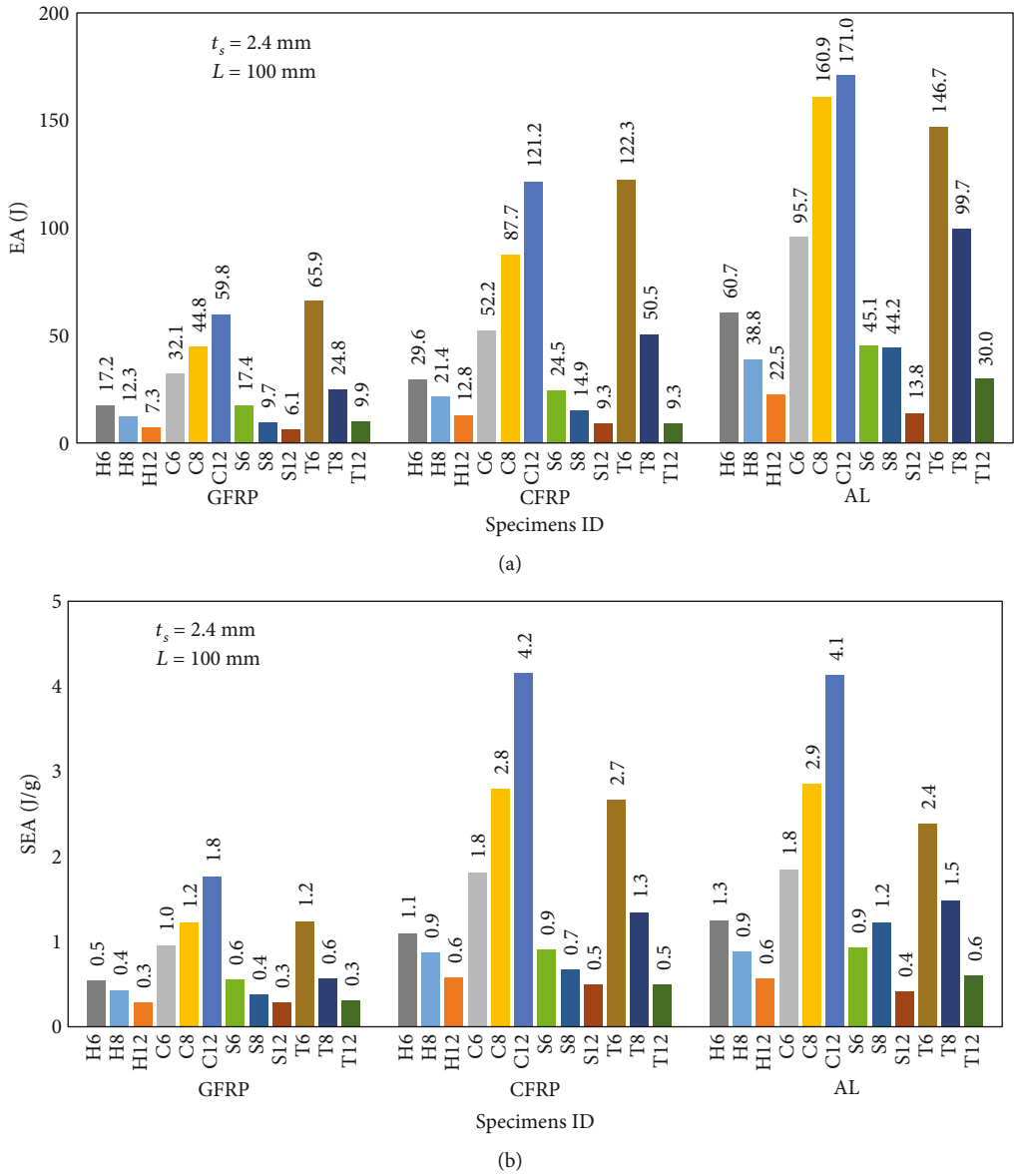

Figure 10: Energy results after compression test: (a) energy absorption (EA); (b) specific energy absorption (SEA).

deviation in linear behavior is observed until the peak. At this point, the structure can resist up to a certain load before a sharp drop in load occurs. Then, a sharp drop in load occurs in the structure. This is the scenario that generally occurs when any specimen is tested in compression [41]. Depending on the type of specimen used, the PCF value and the average load amount with sudden load drop may vary. When Figure 12 is examined, it is observed that for the hexagonal lattice structure, the hexagonal shape shrinks, and shrinkage occurs under the effect of compression force. It is observed that all four different specimens were subjected to global buckling in the first stage of loading with compression load, followed by local buckling and material damage at different locations. Especially in the circular structure, the first deformation occurred at the thinnest point between the two cells due to stress intensity. This is shown in red color in the finite elements. These structures can be locally or globally deformed depending on the geometric parameters. The locations of the initial damage and the deformation patterns depend on the cell structure As the force continued to be applied, first local buckling and then [39, 42] global buckling occurred with the effect of force. For the hexagonal lattice structure, global buckling occurred at an angle of approximately 30 degrees near the top plate. With the increase in force, the specimen folds at the place where global buckling occurs and at this angle. This loading continues until 75% of the total length is deformed. The maximum resistance is shown for the first damage [42].

In case of subsequent loading, the stability of the structure deteriorates and the average force value becomes significantly lower compared to the initial PF value. When the compression [39] behavior of the circular lattice structure is examined, it is observed that the circular structures shrink and shape change occurs as if subjected to shear force. Due

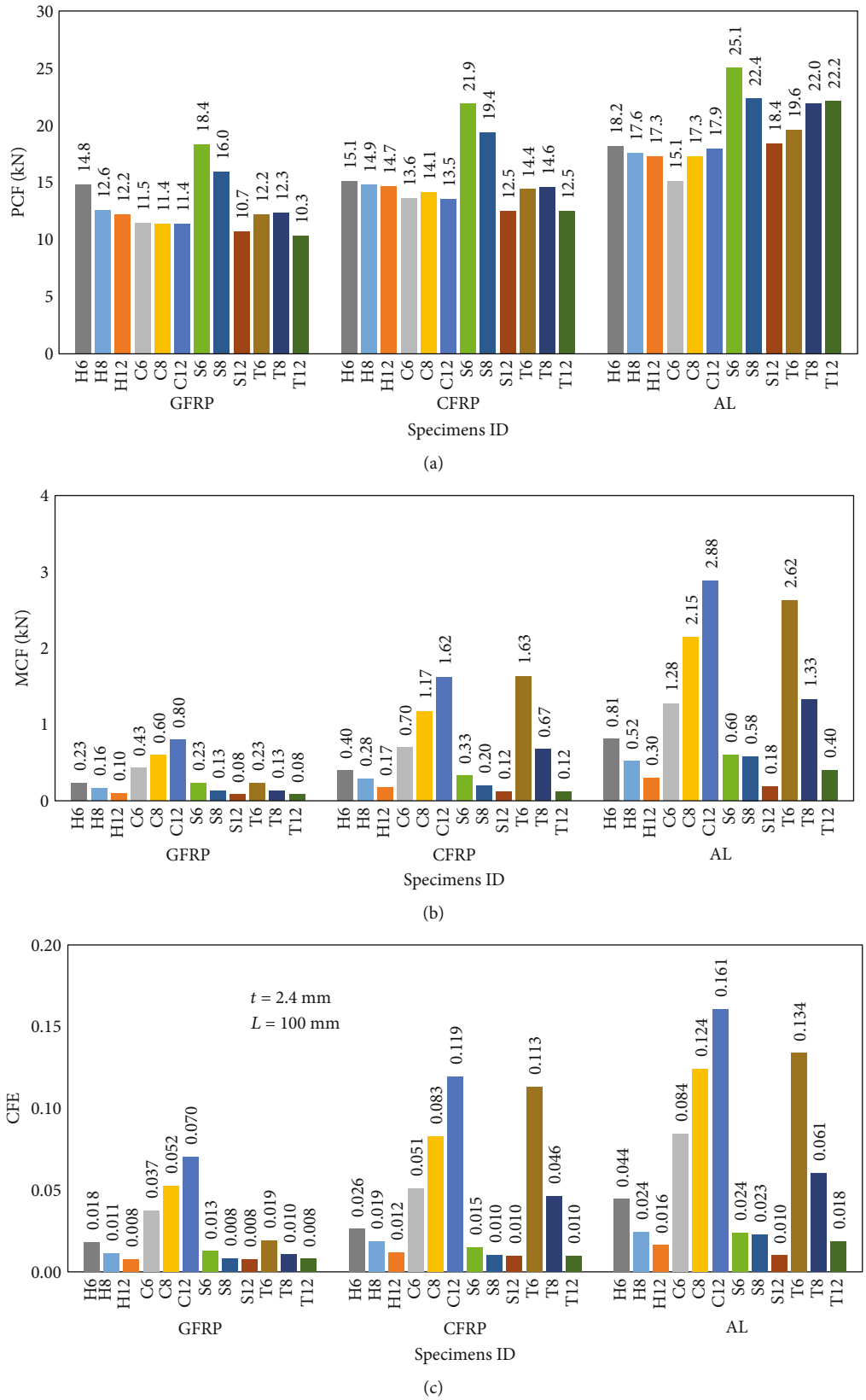

Figure 11: Comparison of peak force values. (a) Peak crushing force (PCF). (b) Mean crushing force (MCF). (c) Crushing force efficiency (CFE).

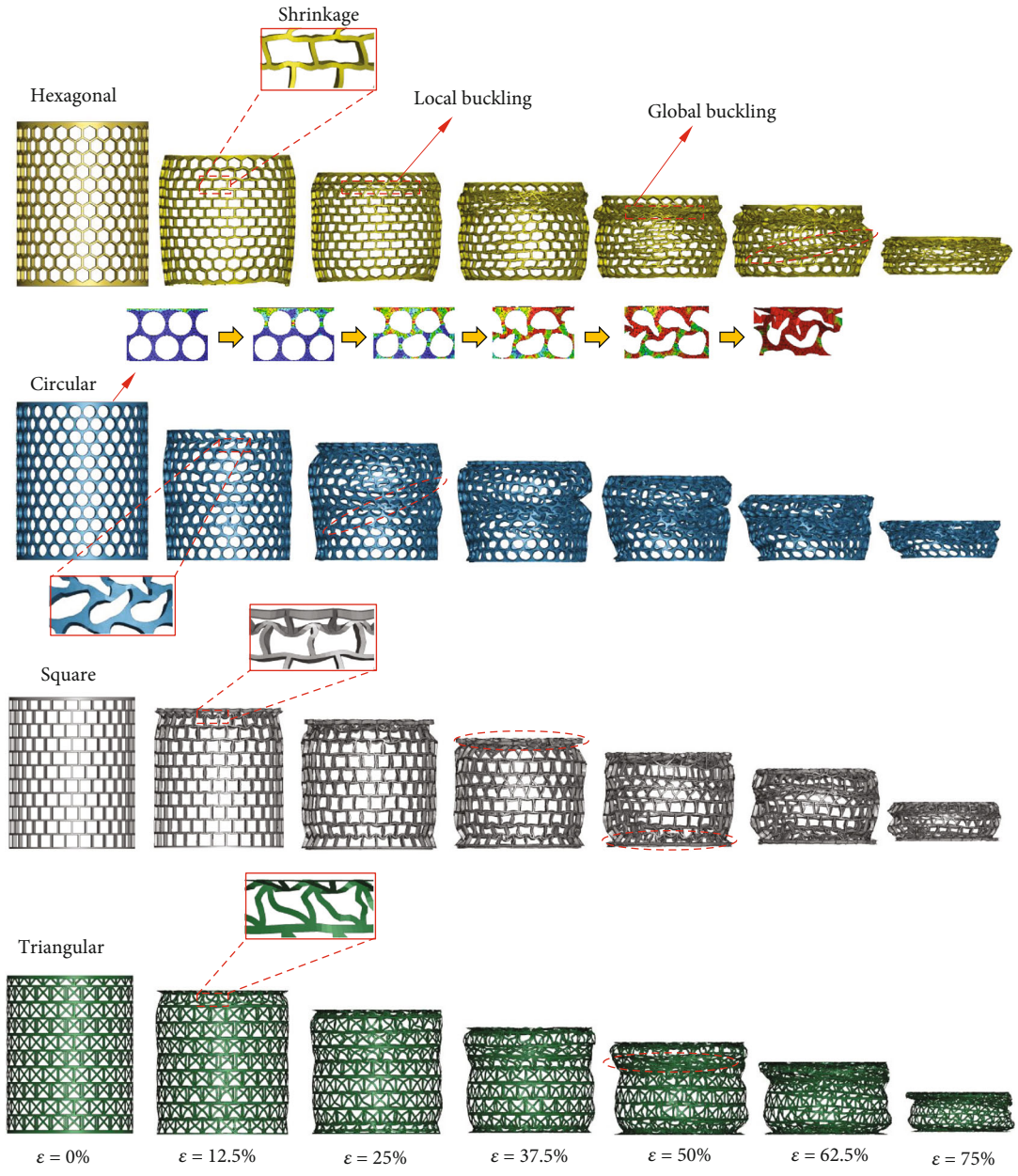

Figure 12: Deformations of lattice structures under compression load.

to the effect of the compression load, shrinkage occurs in the cells, causing the radius of the middle area of the lattice structure to decrease, and the structures become indented inward. As crushing progresses, numerous shear bands form on the surface of the structures, accompanied by the bending of the cells. Over time, the circular cells fill almost the entire structure, and eventually, the cells are twisted until they condense. Under the effect of this densification, the force value in the structure increases [39]. In a square lattice structure, the square structure of the cell structure is disrupted by the compression effect, and the first deformation occurs very close to the top and bottom plates. As the crushing progresses, the structure is damaged in this direction. In the triangular lattice structure, similar to the square lattice structure, it is observed that folds occur close to the upper and lower plate points.

Nowadays, especially in the aerospace industry, the need for lighter and high-strength structures is more and more in demand. For this, researchers have focused on the performance of specimens of different structures under dynamic loading conditions using different material compositions. SEA value is an important criterion, especially in sectors where EA performance is important. The relative density-SEA values of composite lattice cylinder structures under compressive loading are given in Figure 13. The results of the present study are compared with the results in the literature [[17, 43–49]]. When the graph is examined, the SEA value of the circular CFRP lattice structure is 56.7% higher

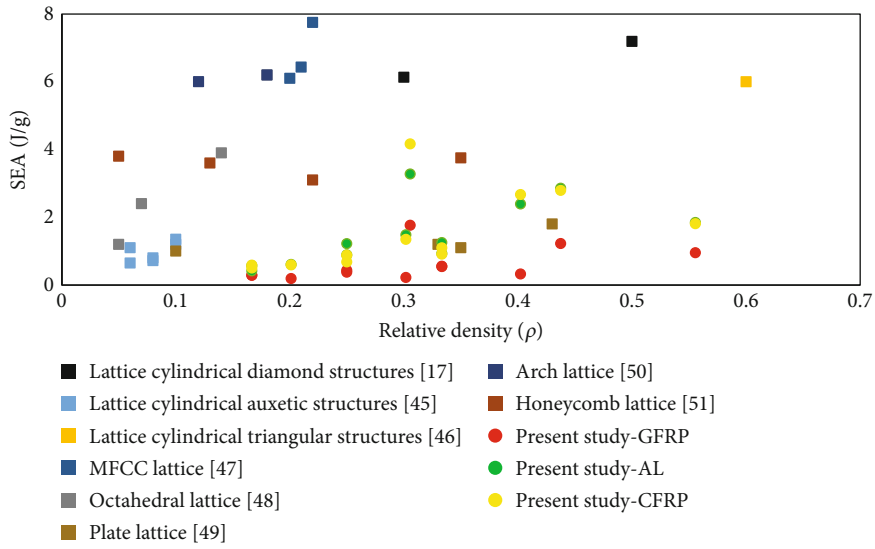

Figure 13: Comparison of SEA values with studies in the literature.

than the honeycomb lattice [49] structure with approximately the same relative density ratio, while it is 72% less than the lattice cylinder diamond [17] structure. The desired situation in sandwich structures is to have a low relative density value and a high SEA value. An important feature that sandwich structures offer to users is that they are optional in this way. In other words, it can be specially selected according to the area of use and the type of component to be used. But ultimately, the main goal is to get maximum efficiency within the safety and cost limits.

4. Conclusions

In this study, the crushing performance of different composite lattice cylinder structures (hexagonal, circular, square, and triangular) under quasistatic compression loading was determined using the finite element method. The numerical model was applied by performing progressive damage analysis with *MAT-54* material model in *LS DYNA* finite element model. In the study, the crushing performance and the types of damage that occurred were determined. Based on the data obtained at the end of the study, the results can be summarized as follows.

For the axial loading case, the PCF value of a square lattice structure is 19.3% higher than hexagonal, 37.6% higher than circular, and 33.4% higher than triangular lattice structure. For the axial loading case, when the cell length used in the lattice structures is increased from $L = 6$ mm to 12 mm, the PCF value decreases by 14.9% for hexagonal, 0.41% for circular, 41.6% for square, and 15.43% for triangular structure. Cell length has a significant effect on PCF. For the tangential loading case, the PCF value of triangular is 55.2% higher than square, 3.1% higher than circular, and 39.5% higher than hexagonal lattice structure. When the cell length was increased from $L = 6$ mm to 12 mm, the triangular lattice structure showed the highest change in PCF value with 55.8%.

When the specimen length increased from $L = 50$ mm to 200 mm, the PCF value decreased by 19.2% for hexagonal lattice, 19.6% for circular lattice, 11.3% for square lattice, and 20.8% for triangular lattice structure. The highest PCF value occurred in the S6-L50 lattice structure with 19.6 kN. When compression test was applied for GFRP, CFRP, and AL cylinder lattice structures, the S6-AL specimen had the highest PCF value with 25 kN. The PCF value increases as the specimen thickness increases. The highest PCF value occurred in specimen H8-4.8 with 21.3 kN. The C12-AL specimen had the highest EA value with 171 J, while the C12-CFRP specimen had the highest SEA value with 4.2 J/g. The CFE value was the highest in the C12-AL specimen. The deformation behavior of latticed cylinders varies mainly according to the cell type. Buckling shape, shrinkage type, and bending angle vary according to the cell structure. This study has a high potential to contribute to the literature if supported by experimental studies in future research.

Data Availability Statement

The data that support the findings of this study are available from the corresponding author upon reasonable request.

Conflicts of Interest

The author declares no conflicts of interest.

Funding

No funding was received for this manuscript.

References

[1] J. Xiong, A. Vaziri, L. Ma, J. Papadopoulos, and L. Wu, "Compression and impact testing of two-layer composite pyramidal-core sandwich panels," *Composite Structures*, vol. 94, no. 2, pp. 793–801, 2012.

[2] M. Albayrak, M. O. Kaman, and I. Bozkurt, "Experimental and numerical investigation of the geometrical effect on low velocity impact behavior for curved composites with a rubber interlayer," *Applied Composite Materials*, vol. 30, no. 2, pp. 507–538, 2023.

[3] M. Hajjari, R. Jafari Nedoushan, T. Dastan, M. Sheikhzadeh, and W. R. Yu, "Lightweight weft-knitted tubular lattice composite for energy absorption applications: an experimental and numerical study," *International Journal of Solids and Structures*, vol. 213, pp. 77–92, 2021.

[4] H. L. Fan, F. N. Jin, and D. N. Fang, "Nonlinear mechanical properties of lattice truss materials," *Materials and Design*, vol. 30, no. 3, pp. 511–517, 2009.

[5] Q. Zheng, D. Jiang, C. Huang, X. Shang, and S. Ju, "Analysis of failure loads and optimal design of composite lattice cylinder under axial compression," *Composite Structures*, vol. 131, pp. 885–894, 2015.

[6] H. L. Fan, F. H. Meng, and W. Yang, "Mechanical behaviors and bending effects of carbon fiber reinforced lattice materials," *Archive of Applied Mechanics*, vol. 75, no. 10–12, pp. 635–647, 2006.

[7] H. L. Fan, D. N. Fang, and F. N. Jing, "Yield surfaces and micro-failure mechanism of block lattice truss materials," *Materials and Design*, vol. 29, no. 10, pp. 2038–2042, 2008.

[8] H. L. Fan, F. H. Meng, and W. Yang, "Sandwich panels with Kagome lattice cores reinforced by carbon fibers," *Composite Structures*, vol. 81, no. 4, pp. 533–539, 2007.

[9] H. L. Fan, T. Zeng, D. N. Fang, and W. Yang, "Mechanics of advanced fiber reinforced lattice composites," *Acta Mechanica Sinica/Lixue Xuebao*, vol. 26, no. 6, pp. 825–835, 2010.

[10] I. Bozkurt, M. O. Kaman, and M. Albayrak, "Low-velocity impact behaviours of sandwiches manufactured from fully carbon fiber composite for different cell types and compression behaviours for different core types," *Materialpruefung/Materials Testing*, vol. 65, no. 9, pp. 1349–1372, 2023.

[11] S. Yu, X. Yu, Y. Ao et al., "The impact resistance of composite Y-shaped cores sandwich structure," *Thin-Walled Structures*, vol. 169, article 108389, 2021.

[12] J. Liu, J. Liu, J. Mei, and W. Huang, "Investigation on manufacturing and mechanical behavior of all-composite sandwich structure with Y-shaped cores," *Composites Science and Technology*, vol. 159, pp. 87–102, 2018.

[13] Q. Wu, X. Liu, J. Li et al., "Failure of carbon fiber composite sandwich cylinders with a lattice core under axial compressive loading," *Composites Part A: Applied Science and Manufacturing*, vol. 155, article 106812, 2022.

[14] P. B. Su, B. Han, M. Yang et al., "Axial compressive collapse of ultralight corrugated sandwich cylindrical shells," *Materials and Design*, vol. 160, pp. 325–337, 2018.

[15] W. Liu, S. Wang, J. Bu, and X. Ding, "An analytical model for the progressive failure prediction of reinforced thermoplastic pipes under axial compression," *Polymer Composites*, vol. 42, no. 6, pp. 3011–3024, 2021.

[16] T. A. Sebeay and A. Ahmed, "Numerical Investigation into GFRP Composite Pipes under Hydrostatic Internal Pressure," *Polymers*, vol. 15, no. 5, p. 1110, 2023.

[17] H. Zhu, P. Wang, D. Wei, J. Si, and Y. Wu, "Energy absorption of diamond lattice cylindrical shells under axial compression loading," *Thin-Walled Structures*, vol. 181, article 110131, 2022.

[18] R. Rafiee and A. Ghorbanhosseini, "Experimental and theoretical investigations of creep on a composite pipe under compressive transverse loading," *Fibers and Polymers*, vol. 22, no. 1, pp. 222–230, 2021.

[19] L. Gemi, M. A. Köroğlu, and A. Ashour, "Experimental study on compressive behavior and failure analysis of composite concrete confined by glass/epoxy ±55° filament wound pipes," *Composite Structures*, vol. 187, pp. 157–168, 2018.

[20] Y. Zhang, Z. Xue, L. Chen, and D. Fang, "Deformation and failure mechanisms of lattice cylindrical shells under axial loading," *International Journal of Mechanical Sciences*, vol. 51, no. 3, pp. 213–221, 2009.

[21] M. Hao, Y. Hu, B. Wang, and S. Liu, "Mechanical behavior of natural fiber-based isogrid lattice cylinder," *Composite Structures*, vol. 176, pp. 117–123, 2017.

[22] W. Li, F. Sun, P. Wang, H. Fan, and D. Fang, "A novel carbon fiber reinforced lattice truss sandwich cylinder: fabrication and experiments," *Composites. Part A, Applied Science and Manufacturing*, vol. 81, pp. 313–322, 2016.

[23] J. Xiong, R. Ghosh, L. Ma, A. Vaziri, Y. Wang, and L. Wu, "Sandwich-walled cylindrical shells with lightweight metallic lattice truss cores and carbon fiber-reinforced composite face sheets," *Composites. Part A, Applied Science and Manufacturing*, vol. 56, pp. 226–238, 2014.

[24] H. Golivari, H. Saeidi Googarchin, A. Zaeri, and A. Keshavarzi, "Experimental and numerical investigation of the energy absorption in hybrid double-hat thin-walled structures reinforced by adhesive bonding under three-point bending," *International Journal of Adhesion and Adhesives*, vol. 128, article 103543, 2024.

[25] A. Mahmoodi, M. H. Shojaeefard, and H. Saeidi Googarchin, "Theoretical development and numerical investigation on energy absorption behavior of tapered multi-cell tubes," *Thin-Walled Structures*, vol. 102, pp. 98–110, 2016.

[26] H. Saeidi Googarchin, M. Pasandidehpoor, A. Mahmoodi, and M. H. Shojaeefard, "Energy absorption analysis for tapered multi-cell tubes improved by foams: theoretical development and numerical simulation," *Composite Structures*, vol. 207, pp. 213–222, 2019.

[27] A. Khorasani and H. Saeidi Googarchin, "Theoretical development and numerical analysis on the energy absorption of tapered multi-cell automotive structures under oblique impacts," *Mechanics Based Design of Structures and Machines*, vol. 51, no. 2, pp. 1016–1034, 2021.

[28] Z. Li, Y. Gao, P. Xue et al., "Fabrication and failure mechanisms of all-composite honeycomb sandwich cylinder under the axial compression," *Composites Part A: Applied Science and Manufacturing*, vol. 161, article 107075, 2022.

[29] Z. Zhang, W. Sun, Y. Zhao, and S. Hou, "Crashworthiness of different composite tubes by experiments and simulations," *Composites Part B: Engineering*, vol. 143, pp. 86–95, 2018.

[30] H. Jo, *LS-DYNA Keyword User's Manual Volume II Material Models, Version 971*, Livermore Software Technology Corporation, 2017.

[31] M. Albayrak, M. O. Kaman, and I. Bozkurt, *Determination of LS-DYNA MAT162 Material Input Parameters for Low Velocity Impact Analysis of Layered Composites*, Researchgate, Paris France, 2022.

[32] P. Feraboli, B. Wade, F. Deleo, M. Rassaian, M. Higgins, and A. Byar, "LS-DYNA MAT54 modeling of the axial crushing of a composite tape sinusoidal specimen," *Composites. Part A, Applied Science and Manufacturing*, vol. 42, no. 11, pp. 1809–1825, 2011.

[33] A. Cherniaev, C. Butcher, and J. Montesano, "Predicting the axial crush response of CFRP tubes using three damage-based constitutive models," *Thin-Walled Structures*, vol. 129, pp. 349–364, 2018.

[34] A. Rabiee and H. Ghasemnejad, "Finite element modelling approach for progressive crushing of composite tubular absorbers in LS-DYNA: review and findings," *Journal of Composites Science*, vol. 6, no. 1, p. 11, 2022.

[35] L. Yuan, C. Wang, Q. Luo, and N. Chen, "Collapse pressure prediction of mechanically lined pipes using FEM and machine learning techniques," *Ocean Engineering*, vol. 268, article 113418, 2023.

[36] N. Chi Tho, D. Van Thom, P. Hong Cong, A. M. Zenkour, D. Hong Doan, and P. Van Minh, "Finite element modeling of the bending and vibration behavior of three-layer composite plates with a crack in the core layer," *Composite Structures*, vol. 305, article 116529, 2023.

[37] M. Albayrak, M. O. Kaman, and I. Bozkurt, "The effect of lamina configuration on low-velocity impact behaviour for glass fiber/rubber curved composites," *Journal of Composite Materials*, vol. 57, no. 11, pp. 1875–1908, 2023.

[38] S. Park, B. P. Russell, V. S. Deshpande, and N. A. Fleck, "Dynamic compressive response of composite square honeycombs," *Composites. Part A, Applied Science and Manufacturing*, vol. 43, no. 3, pp. 527–536, 2012.

[39] X. Zhu, C. Xiong, J. Yin et al., "Experimental study and modeling analysis of planar compression of composite corrugated, lattice and honeycomb sandwich plates," *Composite Structures*, vol. 308, article 116690, 2023.

[40] I. Bozkurt, M. O. Kaman, and M. Albayrak, "Experimental and numerical impact behavior of fully carbon fiber sandwiches for different core types," *Journal of the Brazilian Society of Mechanical Sciences and Engineering*, vol. 46, no. 5, p. 318, 2024.

[41] F. Taheri-Behrooz, R. A. Esmaeel, and F. Taheri, "Response of perforated composite tubes subjected to axial compressive loading," *Thin-Walled Structures*, vol. 50, no. 1, pp. 174–181, 2012.

[42] S. Hou, S. Zhao, L. Ren, X. Han, and Q. Li, "Crashworthiness optimization of corrugated sandwich panels," *Materials and Design*, vol. 51, pp. 1071–1084, 2013.

[43] Y. Guo, J. Zhang, L. Chen et al., "Deformation behaviors and energy absorption of auxetic lattice cylindrical structures under axial crushing load," *Aerospace Science and Technology*, vol. 98, article 105662, 2020.

[44] W. Zhao, T. Liu, L. Chen et al., "Influence of density gradient and hybrid effect on quasi-static axial crushing behavior of lattice cylindrical structures," *Thin-Walled Structures*, vol. 186, article 110720, 2023.

[45] P. Wang, F. Yang, P. Li, B. Zheng, and H. Fan, "Design and additive manufacturing of a modified face-centered cubic lattice with enhanced energy absorption capability," *Extreme Mechanics Letters*, vol. 47, article 101358, 2021.

[46] S. S. S. S. McKown, Y. Shen, W. K. Brookes et al., "The quasi-static and blast loading response of lattice structures," *International Journal of Impact Engineering*, vol. 35, no. 8, pp. 795–810, 2008.

[47] J. J. Andrew, J. Schneider, J. Ubaid, R. Velmurugan, N. K. Gupta, and S. Kumar, "Energy absorption characteristics of additively manufactured plate-lattices under low- velocity impact loading," *International Journal of Impact Engineering*, vol. 149, article 103768, 2021.

[48] R. Ding, J. Yao, B. Du, L. Zhao, and Y. Guo, *Mechanical properties and energy absorption capability of ARCH lattice structures manufactured by selective laser melting*, Wiley-VCH, Verlag, 2020.

[49] B. G. Compton and J. A. Lewis, "3D-printing of lightweight cellular composites," *Advanced Materials*, vol. 26, no. 34, pp. 5930–5935, 2014.